Clim Dyn (2014) 42:941–955
DOI 10.1007/s00382-013-1897-3

Sensitivity of Arctic warming to sea surface temperature distribution over melted sea-ice region in atmospheric general circulation model experiments

Sang-Yoon Jun · Chang-Hoi Ho · Baek-Min Kim · Jee-Hoon Jeong

Received: 24 September 2012 / Accepted: 23 July 2013 / Published online: 6 August 2013

Abstract Substantial reduction in Arctic sea ice in recent decades has intensified air-sea interaction over the Arctic Ocean and has altered atmospheric states in the Arctic and surrounding high-latitude regions. This study has found that the atmospheric responses related to Arctic sea-ice melt in the cold season (October–March) depend on sea-ice fraction and are very sensitive to in situ sea surface temperature (SST) from a series of atmospheric general circulation model (AGCM) simulations in which multiple combinations of SSTs and sea-ice concentrations are prescribed in the Arctic Ocean. It has been found that the amplitude of surface warming over the melted sea-ice region is controlled by concurrent in situ SST even if these simulations are forced by the same sea-ice concentration. Much of the sensitivity of surface warming to in situ SST are related with large changes in surface heat fluxes such as the outgoing long-wave flux in early winter (October–December) and the sensible and latent heat fluxes for the entire cold season. Vertical extension of surface warming and moistening is sensitive to these changes as well; the associated condensational heating modulates a static stability in the lower troposphere. This study also indicates that changes in SST fields in AGCM simulations must be implemented with extra care, especially in the melted sea-ice region in the Arctic. The statistical method introduced in this study for adjusting SSTs in conjunction with a given sea-ice change can help to model the atmospheric response to sea-ice loss more accurately.

Keywords Arctic warming · General circulation model · Sea-ice · Melting · Surface heat flux

S.-Y. Jun · C.-H. Ho
School of Earth and Environmental Sciences, Seoul National University, Seoul, Korea

B.-M. Kim (✉)
Korea Polar Research Institute, Inchon 406-840, Korea
e-mail: bmkim@kopri.re.kr

J.-H. Jeong
Faculty of Earth Systems and Environmental Sciences, Chonnam National University, Gwangju, Korea

1 Introduction

Melting of Arctic sea ice has been greatly accelerated in recent decades. The sea-ice extent in September 2007 was 37 % lower than its climatology (Comiso et al. 2008), and the 5-year mean for 2006–2010 reached the record minimum value (Stroeve et al. 2012). The historical reconstructed data of Arctic sea ice shows that the current decline is unprecedented, at least for past 1,450 years (Kinnard et al. 2011). Anthropogenic forcing is regarded as a primary cause of this tremendous sea-ice decline. It is suggested that both local climate feedbacks (e.g., ice-albedo feedback) and heat transfer from mid-latitudes have reinforced the decline (IPCC 2007; Screen and Simmonds 2010a; Stroeve et al. 2012; Winton et al. 2010).

The reduction of Arctic sea ice, particularly in the areal extent (i.e., the increase of open ocean area occupied by water surface), is known to greatly amplify local warming in the Arctic during the boreal winter (Screen and Simmonds 2010b) through large increases in sensible and latent heat fluxes from the ocean surface areas of below normal ice coverage. This mechanism is the main cause of Arctic amplification (Screen and Simmonds 2010a, b) in conjunction with enhanced northward energy transport from the mid-latitudes to the Arctic (Chung and Räisänen 2011; Graversen et al. 2008). In addition, considerable surface

warming destabilizes and moistens the lower troposphere—these result in the increased condensation to form additional overlying mid-level clouds (Schweiger et al. 2008). Surface warming contributes to the thickening of the Arctic lower troposphere as well, to affect winter weather patterns and large-scale atmospheric circulations over the mid-latitudes (Francis et al. 2009; Overland and Wang 2010).

Many previous studies have investigated the impact of Arctic sea ice on large-scale environments over the Northern Hemisphere using atmospheric general circulation models (AGCMs) (Budikova 2009). These studies have focused mainly on the atmospheric sensitivity to the changes in sea-ice extent. In early 1970s, several studies examined the atmospheric response to a complete removal of Arctic sea ice (Newson 1973; Warshaw and Rapp 1973). A modeling study by Herman and Johnson (1978) demonstrated that changes in Arctic ice-cover can influence large-scale atmospheric circulations as far south as in the subtropics by modifying the latitudinal temperature gradient. Murray and Simmonds (1995) performed a perpetual January simulation by gradually reducing sea-ice coverage; their results suggest that Arctic sea-ice extent is non-linearly related to the changes in the 850 hPa temperature over the Arctic and mid-latitude westerlies.

Alexander et al. (2004) correlated large-scale atmospheric teleconnection patterns, such as the Arctic Oscillation/North Atlantic Oscillation (AO/NAO), to anomalous sea-ice cover. Deser et al. (2004) investigated an AO/NAO-type atmospheric response to changes in North Atlantic sea ice and sea surface temperature (SST) conditions based on observations spanning over a 40-year period. Singarayer et al. (2005) performed a climate model simulation with observed sea-ice distributions for 1980–2000 and found that the decline of sea ice is linked to the NAO positive phase during the winters of late 1980s and early 1990s. Screen et al. (2012) suggested that the response pattern of atmospheric circulation in early winter to sea-ice loss in the last three decades resembles the NAO negative phase. This NAO-type atmospheric response is also found in future climate projections under reduced Arctic sea-ice conditions (Deser et al. 2010; Seierstad and Bader 2009).

Arctic atmospheric response to local changes in sea-ice conditions is quite sensitive and non-linear (Singarayer et al. 2005). To account for this sensitivity, researchers have been specifying more detailed and observation-based sea-ice conditions in AGCM experiments. For instance, both the thickness and fractional coverage of sea ice are used to specify surface boundary conditions (Gerdes 2006; Rind et al. 1995). Dethloff et al. (2006) achieved a realistic surface air temperature (SAT) simulation for the Arctic using an improved sea-ice albedo scheme.

Changes in sea-ice concentration (SIC) are a primary factor in driving atmospheric changes by inducing dramatic changes in energy and moisture exchanges between the sea surface and the lower troposphere. Based on this, a number of previous studies have investigated atmospheric responses to altered SIC (Alexander et al. 2004; Magnusdottir et al. 2004; Semmler et al. 2012; Singarayer et al. 2006). Typically, SST in the melted sea-ice region (MSR) is estimated by using SST values at the adjacent grids (Alexander et al. 2004) or by using sea-ice surface temperature (Semmler et al. 2012); none of earlier studies use SIC fraction in the estimation of the SST over MSR.

This earlier approach in estimating SSTs in MSR is rather unrealistic and may produce erroneous results. As the sea ice and ocean interact, their changes are always concurrent. For instance, the heat absorbed by the Arctic Ocean when covered with broken sea ice is used in part to melt sea ice and in part to increase SST. Thus, the oceanic area exhibiting significant reduction in SIC is expected to show a significant increase in local SST. Because heat fluxes between two interfaces (i.e., atmosphere and ocean surface) increase the temperature difference between the two interfaces; the increased SST provides more heat and moisture fluxes into the lower troposphere. Hence, accurate determination of local SST in a region where SIC exhibits dramatic decreases is essential for improving the simulations in sea-ice model experiments.

This study shows that the atmospheric response associated with sea-ice variability depends on SIC, and the response is very sensitive to in situ SST distributions. To isolate the atmospheric response to SSTs in a given SIC change, we compare the results from multiple AGCM simulations generated using various SST conditions in MSR. Model configurations for the sensitivity include: (1) no SST change; (2) SST adjusted by averaging a long-term climatology with a constant value for the lowest ice-free SST; and (3) SST from a statistical fitting concurrent with the in situ observed SIC. By comparing the three corresponding sensitivity experiments, we have examined the atmospheric responses during the cold season (October through March) and changes in the associated surface-heat fluxes.

In Sect. 2, we discuss the model and experimental design, including a detailed description of SST adjustment methods. An analysis of model results is presented in Sect. 3. A summary and discussion are provided in Sect. 4.

2 Model and experiments

This study employs the National Center for Atmospheric Research (NCAR) Community Atmospheric Model version 3 (CAM3), the atmospheric component of the NCAR Community Climate System Model version 3 (CCSM3;

Collins et al. 2006). The CCSM3 was used in the Coupled Model Inter-comparison Project phase 3 (CMIP3; Meehl et al. 2007). The version used in this study is configured with a finite volume dynamics core having a 4 × 5° horizontal resolution and 26 vertical levels. Previous studies suggested that the sensitivity of the atmospheric response to surface boundary and doubling-CO_2 conditions in the CAM3 version increases with spatial resolution (Hack et al. 2006; Kiehl et al. 2006). Thus, results from this type of experiment using the model can vary according to the spatial resolutions; relatively low resolution used in this study may give results derived from conditions of relatively lower sensitivity.

To assess atmospheric responses to SST changes in MSR, a series of CAM3 experiments have been performed; one baseline and three sensitivity experiments. The baseline experiment prescribes the monthly climatological seasonal cycles of SST and SIC from the National Oceanic and Atmospheric Administration Optimum Interpolation version 2 (OISSTv2) (Reynolds et al. 2002) for 1982–2000. The three sensitivity runs employ the same reduced SIC averaged over 2006–2010, but with different MSR SST conditions. It is noted that, for the period 2006–2010, there is a dramatic decrease in Arctic sea-ice extent in winter (Stroeve et al. 2012).

In the three sensitivity experiments, MSR is defined as the region where the time-mean SIC for 2006–2010 is reduced by over 1 % compared to that for 1982–2000. Local SSTs are specified over MSR as follows: the first experiment (hereafter CTRL) prescribes the same SST field as in the baseline run in conjunction with the reduced SIC. The second experiment (hereafter CONV) adjusts SST at the MSR grid points using average of the mean climatological SSTs for 1982–2000 and the minimum value of −0.8 °C. This method is designed to follow the conventional approach of Alexander et al. (2004) where the SST in grids adjacent to the sea-ice is constrained with the average of value of −0.8 °C (the lowest ice-free SST) and the warmest climatological SST in adjacent grid boxes. In the third experiment (hereafter POLY), the MSR SSTs are estimated to be more physically associated with the given sea-ice reduction using a statistical relationship between SIC and SST over MSR derived from a 3rd-order polynomial regression method.

Figure 1 presents a scatter plot of the observed relationship between SST and SIC over the ocean, north of 60°N for the cold seasons (October through March) for the period 1982–2000. In general, regions of larger sea-ice cover show relatively colder SSTs, close to the sea-water freezing point (around –1.8 °C); SSTs over areas with

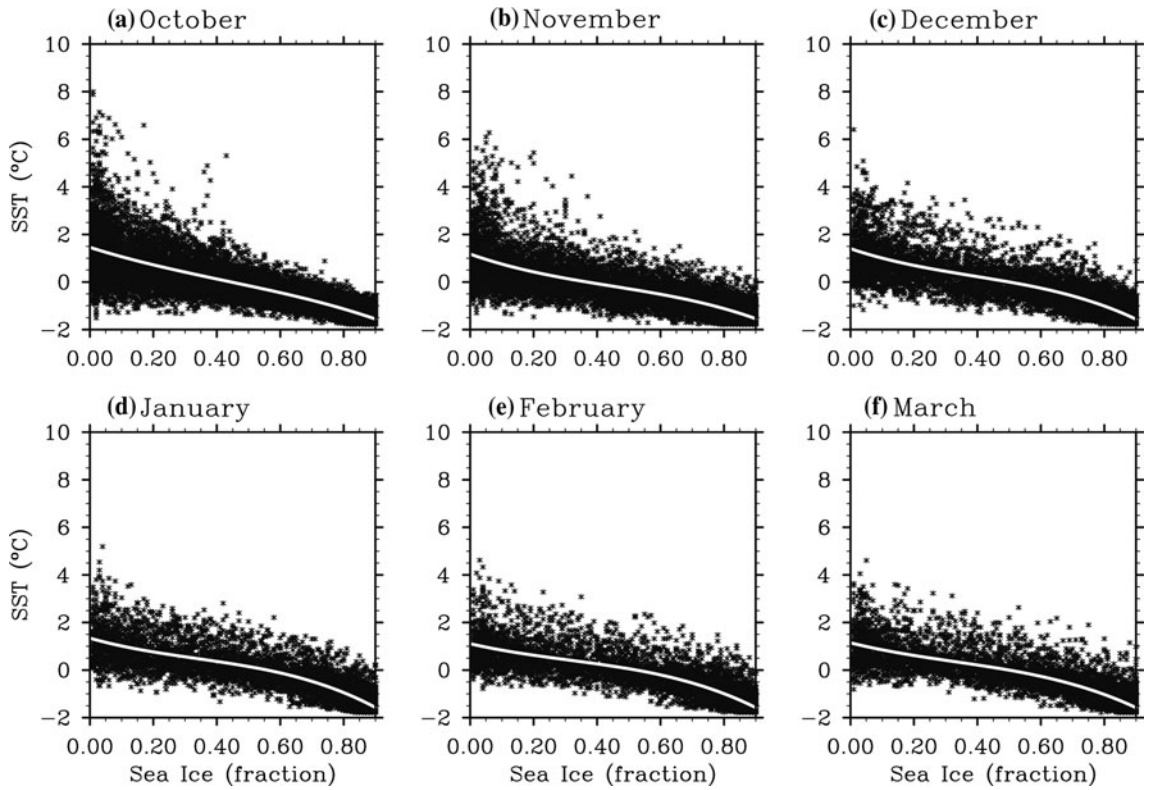

Fig. 1 Scatter plot between sea-ice concentration (SIC; fraction) and sea surface temperature (SST) over the Arctic (north of 60°N) for the cold season (October through March) of the period 1982–2000 from OISST v2. *White lines* indicate the third-degree polynomial fitting between SIC below 0.9 fraction and SST, in each month

Table 1 The 3rd polynomial fitting coefficients for the relationship between SST and sea-ice fraction for each month during the cold season

	Oct	Nov	Dec	Jan	Feb	Mar
a	1.4573	1.1727	1.4012	1.3413	1.1103	1.1486
b	−4.248	−4.716	−4.5208	−3.7716	−3.1089	−3.3505
c	3.3636	5.7375	6.0431	5.4956	4.3157	4.2713
d	−2.626	−4.278	−5.1979	−5.4454	−4.6410	−4.3526

* $y = \mathbf{a} + \mathbf{b}x + \mathbf{c}x^2 + \mathbf{d}x^3 + \varepsilon$ where x and y are sea-ice (fraction) and, SST (°C), respectively, and ε is residual

small sea-ice cover vary widely. White lines in the figure represent a 3rd-degree polynomial fit to the observed data. These polynomials are calculated using data over the regions of SIC < 0.9. SSTs where SIC > 0.9 are excluded as SSTs over such regions are approximately constant (i.e., –1.8 °C). These polynomials represent the seasonal variation reasonably in the relationship between the two variables (SST and SIC). This fitting method is currently applied to adjust bias in the Hadley Centre Sea Ice and Sea Surface Temperature data (HadISST) using a 2nd-degree polynomial to estimate SSTs over MSR where SST observations are absent (Rayner et al. 2003). In our POLY experiment, SSTs over MSR are specified based on the third-degree polynomial fits; the SST corresponding to the given SIC from the fitting line is chosen as the SST over MSR. Table 1 presents the polynomial fitting coefficients between the two variables in the POLY experiment during the cold season.

The baseline and three sensitivity experiments have been run for 250 years by prescribing the annual cycles of SST- and SIC fields corresponding to each experiment as described above. In this study, we focused on the cold season responses when the atmospheric local response to an altered boundary condition is known to be strongest (Screen and Simmonds 2010b; Screen et al. 2012). Table 2 summarizes the monthly-mean values of SST and SIC during the cold season, averaged over the Arctic Ocean to the north of 67°N in all experiments. As expected, among the sensitivity experiments, POLY had mean values of SST for 2006–2010 that are closest to those obtained by the OISSTv2 product. The mean SST in CONV in October is considerably colder than in POLY; the colder SSTs in CONV affects values in autumn and December, perhaps because the method used in CONV is originally designed to model atmospheric response during December–January–February (Alexander et al. 2004).

Figure 2 shows the SIC differences between the sensitivity and baseline experiments (contour in all panels). Also shown are the SST differences in CONV (shading, Fig. 2b, f) and POLY (shading, Fig. 2c, g) from CTRL in early winter (October–December) (Fig. 2a–d) and late winter (January–March) (Fig. 2e–h). Note that SSTs in CONV and POLY are explicitly calculated using the local SIC value. For comparison, the SST changes in OISSTv2 between 2006–2010 and 1982–2000 are presented in (Fig. 2d, h for the corresponding periods. In terms of the pattern and amplitude of SST anomalies, results from POLY are most similar to observations. Compared to POLY, CONV has apparently smaller SST increases over most of MSR. In addition, colder SSTs are generally found in the Barents Sea indicating that CONV is unable to capture the SST changes associated with the recent decline in early and late winter (Fig. 2b, f). Previous studies have noted that SIC changes over the Barents Sea and Kara Sea play a crucial role in modulating large-scale atmospheric circulations (Honda et al. 2009; Petoukhov and Semenov 2010). Thus, these results imply that using SST values adjusted to the lowest SST in the ice-free region cannot generate proper atmospheric responses because warming over the Barents and Kara Seas is much weaker than the observed. More detailed examination of early winter conditions shows that, over most of the Arctic Ocean, POLY captures the SST increase associated with the SIC decrease better than CONV (Fig. 2b, c). However, warming over the Barents Sea in POLY is overestimated compared to the observation (Fig. 2c, d). In late winter, CONV presents excessive warming over the Kara Sea and Laptev Sea (Fig. 2f, h). In contrast, those for POLY in late winter are closer to the observed SST changes associated with the changes in SIC. Still, a stronger warming tendency appears over the Barents Sea (Fig. 2g, h).

3 Results

3.1 Responses in surface air temperature and heat fluxes

We first compare the CTRL with the baseline results to examine the SAT response related solely with changing sea-ice conditions and fixed climatological SST (Fig. 3a). During the cold season, the reduced SIC induces overall warming over the Eurasian margins of the Arctic Ocean and Hudson Bay by more than 1 K, with particularly strong warming over the Barents Sea of approximately 3 K. This spatial variation in SAT response also appears in CONV and POLY. Compared to CTRL, POLY shows stronger the warming over the Barents Sea; both CONV and POLY show further horizontal expansions of warming to the Eurasian margins (Fig. 3b, c). With the same SIC changes, the mean SAT difference between 2006–2010 and 1982–2000 is estimated from the European Center for Medium-Range Weather Forecast Interim Re-Analysis (ERA-Interim; Dee and Uppala 2009). The estimate shows

Table 2 Summary of surface conditions of experiments in this study

Experiment	Sea ice	SST	SST averaged over the Arctic Ocean (north of 67°N, °C)						
			OCT	NOV	DEC	JAN	FEB	MAR	OND JFM
Baseline	Averaged annual cycle for 1982–2000	Averaged annual cycle for 1982–2000	0.10	−0.65	−0.89	−1.01	−1.08	−1.08	−0.77
CTRL	Averaged annual cycle for 2006–2010	Same as baseline	0.10	−0.65	−0.89	−1.01	−1.08	−1.08	−0.77
CONV		Adjusted to average of climatology for 1982–2000 and −0.8 °C	0.10	−0.56	−0.82	−0.93	−1.00	−1.01	−0.70
POLY		Adjusted to the 3rd degree polynomial fitted SST where sea ice fraction is melted to below 0.9	0.47	−0.50	−0.80	−0.92	−1.01	−1.02	−0.63
2006–2010*	Averaged annual cycle for 2006–2010	Averaged annual cycle for 2006–2010	0.38	−0.49	−0.78	−0.88	−0.97	−1.03	−0.63

* Only for comparison

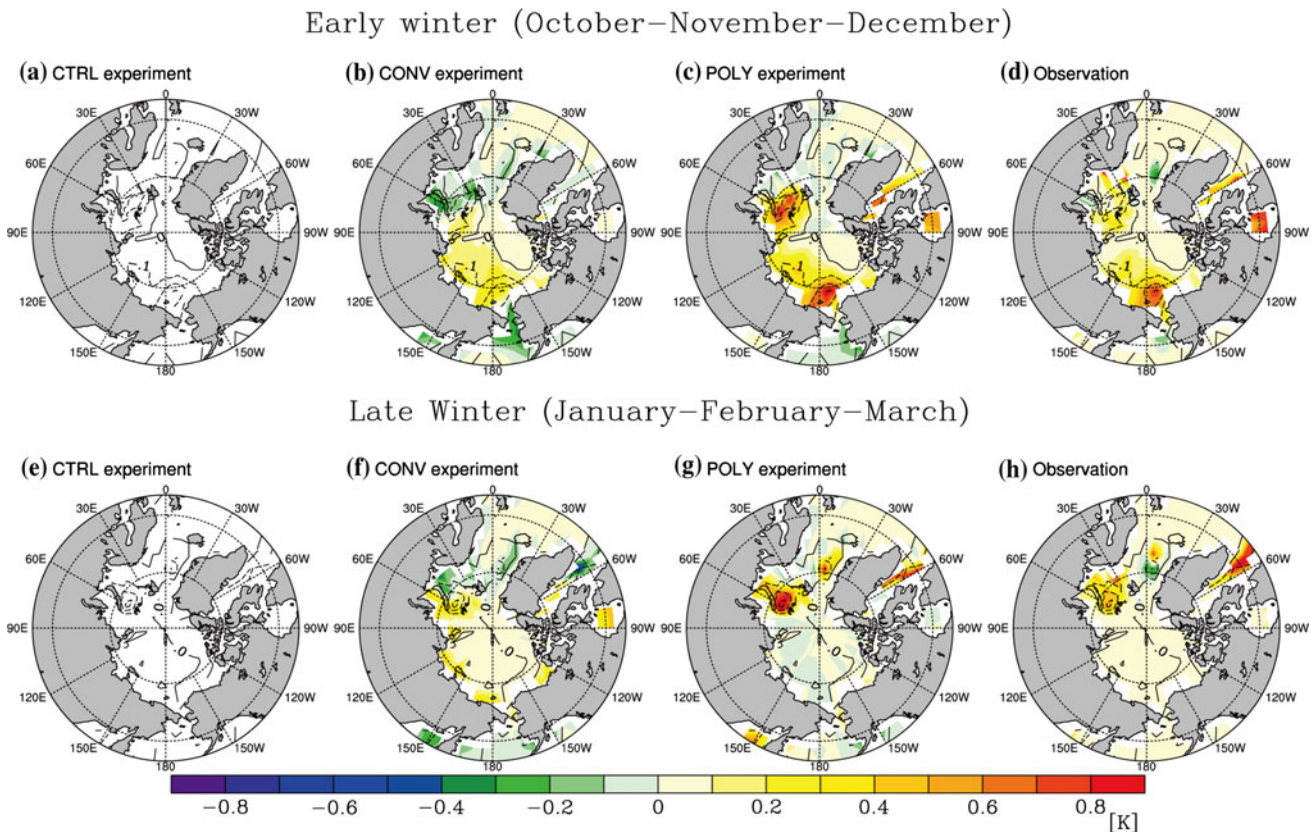

Fig. 2 Differences of sea surface temperature (*shade*) and sea-ice concentration (*contour*) boundary conditions from **a**, **e** CTRL, **b**, **f** CONV, and **c**, **g** POLY experiments compared to the baseline experiment during early winter (October–November–December) and late winter (January–February–March); **d**, **h** Differences between mean sea surface temperature during early and late winters for 2006–2010 and 1982–2000 from the OISST v2. Differences are plotted only over the region where sea-ice reduced above 0.01 fraction. In *all panels*, the contour interval is 0.1 fraction

warming > 3 K over major sea-ice reduced regions and extreme warming > 6 K over the Barents Sea (Fig. 3d). All three experiments yield smaller warming compared to the ERA-Interim data, perhaps due to weaker internal variability since the results obtained in this study is the mean response averaged over much longer period than the averaging period of the ERA-Interim data. In addition, the lack of heat transport from lower latitudes in the three

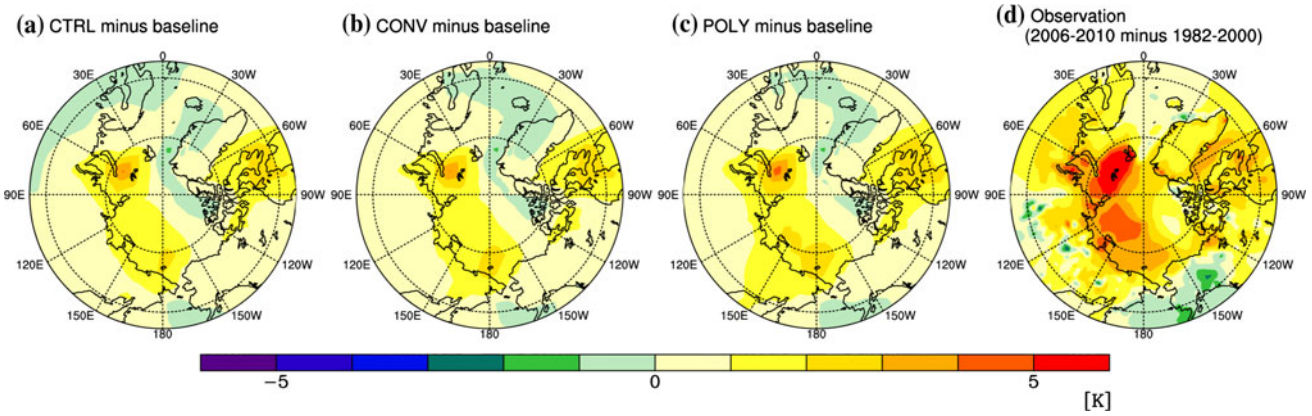

Fig. 3 Change in surface air temperature from **a** CTRL, **b** CONV, **c** POLY compared to the baseline experiment during the cold season, and **d** 2 m air temperature difference between 2006–2010 and 1982–2000 during the cold season from the ERA-Interim data

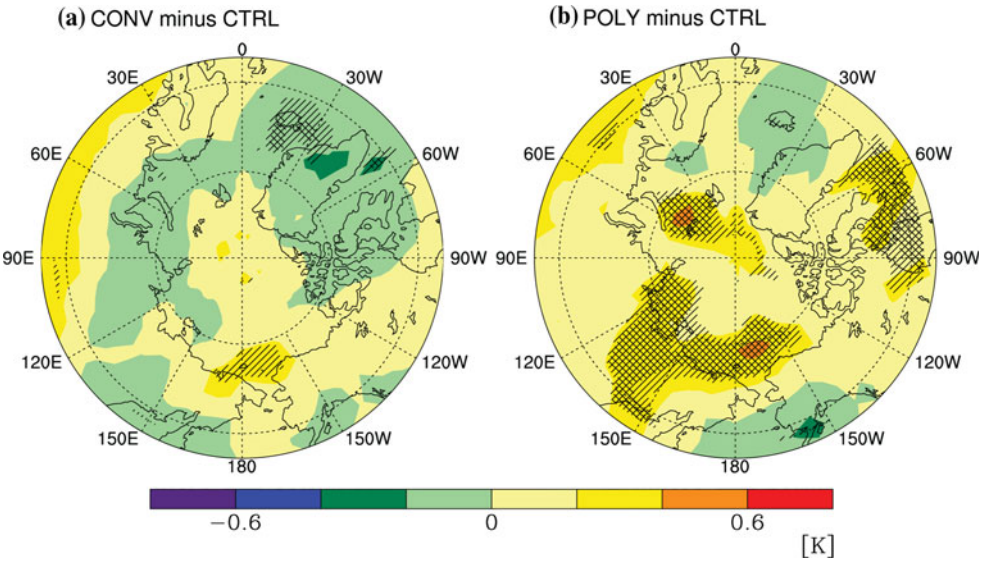

Fig. 4 Change in surface air temperature from **a** CONV and **b** POLY compared to CTRL experiment during the cold season. *Oblique* and *cross regions* indicate that surface air temperature response is significant at the 90 and 95 % confidence level, respectively

sensitivity experiments can be another reason for this weaker warming because they use the climatological SSTs where SIC does not change.

In Fig. 4, we compare SAT responses in CONV and POLY against CTRL. Under the same SIC change, SAT in POLY differs significantly from that in CONV. CONV generates slightly weaker SAT responses compared to CTRL over most of the Arctic Ocean, except for weak warming of about 0.2 K over the Chukchi Sea (Fig. 4a), consistently with the prescribed colder SSTs in the Barents Sea and warmer SSTs in the Chukchi Sea in CONV (Fig. 2b, f). In contrast, POLY generates significant warming of 0.2 K over most of the Arctic Ocean, particularly by as much as 0.4 K over the Barents Sea (Fig. 4b). Considering the changes found in the ERA-Interim reanalysis data, POLY appears to simulate SAT response over the Arctic more reasonably, in both intensity and spatial distribution, than CONV. Even though warming in POLY is weaker than the observed, our results suggest that a careful choice of the SST field based on statistical estimation can improve model response. In addition, the relatively weaker warming found in the experiments, even in POLY, emphasizes that heat transport from lower latitudes is a major cause of Arctic warming (Chung and Räisänen 2011; Graversen et al. 2008).

Screen and Simmonds (2010b) showed that, during the cold season, recent Arctic warming is largely associated with enhanced surface heat fluxes over the region of reduced sea-ice. Here, we examine the changes in surface heat fluxes associated with SST distributions that might be closely associated with SAT responses. CAM3 formulates surface fluxes in the sea-ice covered region as follows (Collins et al. 2004),

$$F_{LWUP} = \varepsilon\sigma_{sb}T_s^4 - (1-\varepsilon)F_{LWDN} \quad (1)$$

$$F_{SH} = \rho_a c_a r_h u^*(T_s - \theta_a) \quad (2)$$

$$F_{LH} = \rho_a(L_i + L_v)r_e u^*(\overline{q}^* - q_a) \quad (3)$$

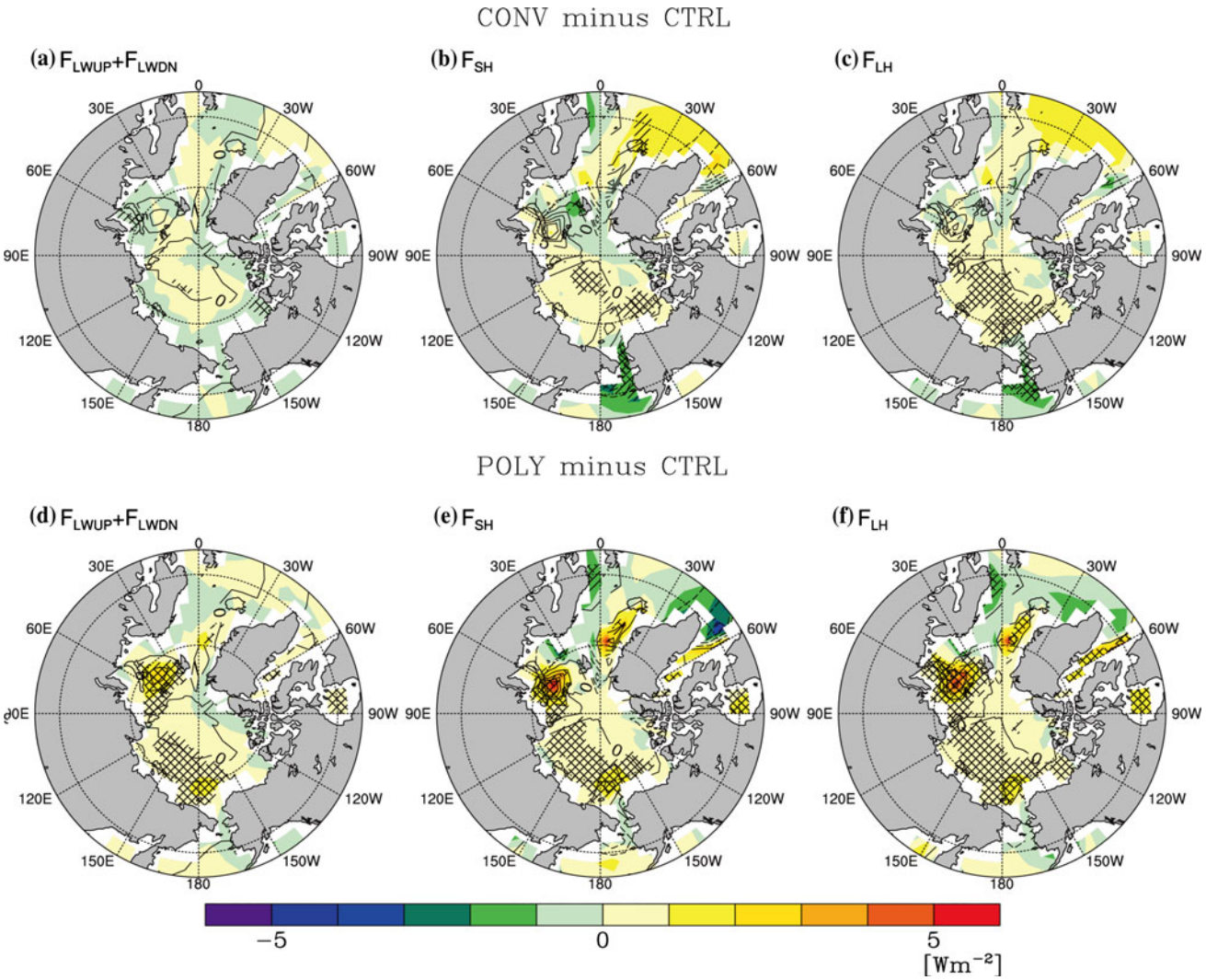

Fig. 5 Changes in net longwave flux (positive in the *upward direction*), sensible heat flux, and latent heat flux at the surface from CTRL (*contour* in all figures) compared to the baseline experiment, and changes in **a–c** CONV and **d–f** POLY experiments compared to CTRL experiment (*shade* in all figure) during the cold season. Contour interval is 5 W m^{-2}. *Oblique* and *cross regions* indicate that surface fluxes are significant at the 90 and 95 % confidence level, respectively

where, the upwelling longwave flux is F_{LWUP}; sensible heat flux is F_{SH}; latent heat flux is F_{LH}; downwelling longwave flux is F_{LWDN}; longwave emissivity is ε; Stefan-Boltzmann constant is σ_{sb}, specific heat of air is c_a, exchange coefficients for sensible and latent heat are r_h and r_e, respectively; and latent heat of fusion of ice and vaporization are L_i and L_v, respectively. At the lowest model layer, the air density is ρ_a; potential temperature is θ_a; and specific humidity q_a. At the surface, the temperature is T_s; friction velocity is u^*; and saturation specific humidity is $\overline{q}^*$. In the equations, all surface fluxes are defined to be positive in upward direction.

When the ocean surface previously occupied by sea ice becomes warmer, MSR experiences a significant increase in surface fluxes. In Fig. 5, all of the SIC change experiments show a consistent increase in surface fluxes over MSR (see contours in the figure). Net longwave flux ($F_{LWUP} + F_{LWDN}$) increases over the Barents Sea, Laptev Sea, and East Siberian Sea; these regions also experience large increases in sensible (F_{SH}) and latent (F_{LH}) heat fluxes. In particular, a large reduction in sea ice over the Barents Sea leads to increases in both sensible and latent heat fluxes. Elsewhere, in the inner-Arctic, especially over the northeast of Greenland and Queen Elizabeth Islands, the sea-ice expanded region undergoes a conspicuous decrease in sensible heat flux of more than 1 W m^{-2}. This occurs in all three experiments (contour in the Fig. 5b, e) due mainly to the cold surface temperatures over the sea-ice expanded region, which are colder than in the baseline experiment.

In CONV and POLY, warmer SSTs increase the outgoing longwave flux as well as the sensible and latent heat

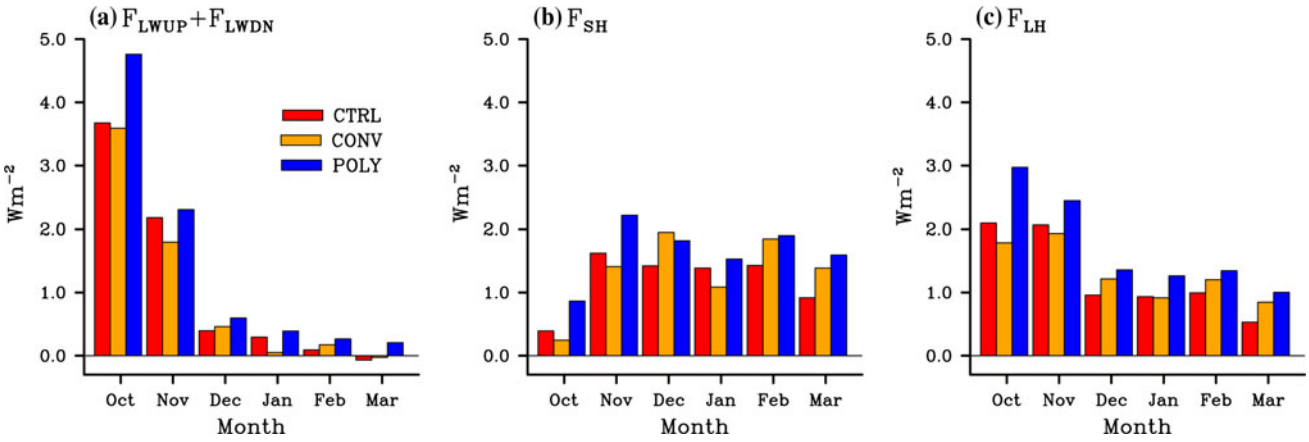

Fig. 6 Monthly changes in **a** net longwave flux (positive in the *upward direction*), **b** sensible heat flux, and **c** latent heat flux averaged over the Arctic Ocean (north of 67°N) from CTRL, CONV, and POLY experiments compared to the baseline experiment

fluxes. Compared to CTRL, POLY shows significant and larger increases in surface fluxes over most MSRs (Fig. 5d–f) than CONV (Fig. 5a–c). These increases in surface fluxes in POLY are roughly proportional to the reduction of sea-ice because fluxes increase most over the Barents Sea and north of the Chukchi Sea and considerably less elsewhere. In particular, increases in the surface fluxes over the Barents Sea were above 3 W m^{-2}. These changes over MSR in POLY are significant at the 95 % confidence level.

The SAT responses obtained in the three experiments are well explained by increases in surface flux changes. Surface flux changes might have different monthly variations due to diverse dependencies of the fluxes on the seasonal evolution of SST. Because longwave flux increases in proportion to the fourth power of SST, as indicated by Eq. (1), an increase in longwave flux becomes larger in early winter than in late winter because the early winter has a considerably warmer SST value. In Fig. 6a, changes in net longwave flux are largest over the Arctic Ocean, exceeding 3.6 W m^{-2}, and represent warmer SST conditions in October. In November, all experiments show a stronger longwave flux, 2 W m^{-2} more than in the baseline experiment. Afterwards, the net longwave flux changes become much weaker as the Arctic becomes colder. Thus, differences among all methods are nearly zero in February and March; the impact of longwave flux is concentrated in the two months, October and November.

Changes in sensible heat flux for all experiments remain in a similar range of 1–2 W m^{-2} in every month, except for October; the change is relatively small in October compared to the changes in other cold months (Fig. 6b). In Eq. (2), sensible heat flux mainly depends on the difference between the potential temperature at the lowest atmospheric level and the surface temperature. The temperature differences in all experiments closely match observed sensible heat fluxes during all cold months. These differences are smallest in October, although SST anomalies in all experiments are largest in October compared to the baseline experiment (not shown).

Among experiments, the sensible heat flux in POLY is consistently larger than that in CTRL during the whole cold season. However, sensible heat flux in CONV is smaller than that in CTRL for several months (Fig. 6b). This feature is coupled tightly to the SST change in MSR, especially over the Barents Sea. The SST in POLY bears a more accurate warming signal, corresponding to a reduction in SIC, while SST in MSR CONV is colder than in CTRL for most periods. This SST difference occurs throughout the entire winter (see Fig. 2) and follows the sensible heat flux difference between CONV and CTRL quite well.

Changes in latent heat flux are more sensitive to changes in SST conditions than are other fluxes throughout the cold season in the models. As shown in Eq. (3), latent heat flux depends mainly on the difference between specific humidity in the lowest layer and saturated specific humidity at the surface. In the annual cycle, both the specific humidity at the lowest model layer and the saturated specific humidity at the surface have maximum values in July and August. However, saturated specific humidity declines more gradually in association with declines of SIC. Consequently, the latent heat flux over the Arctic peaks in October and declines through the remaining cold season (not shown). In addition, because specific humidity in the lowest layer changes least in all three sensitivity experiments, changes in the saturated specific humidity at the surface is more responsible than other factors for increasing latent heat fluxes. Because saturated specific humidity at the surface increases exponentially with SST, different SST distributions in each sensitivity experiments contribute largely to the differences in latent heat fluxes

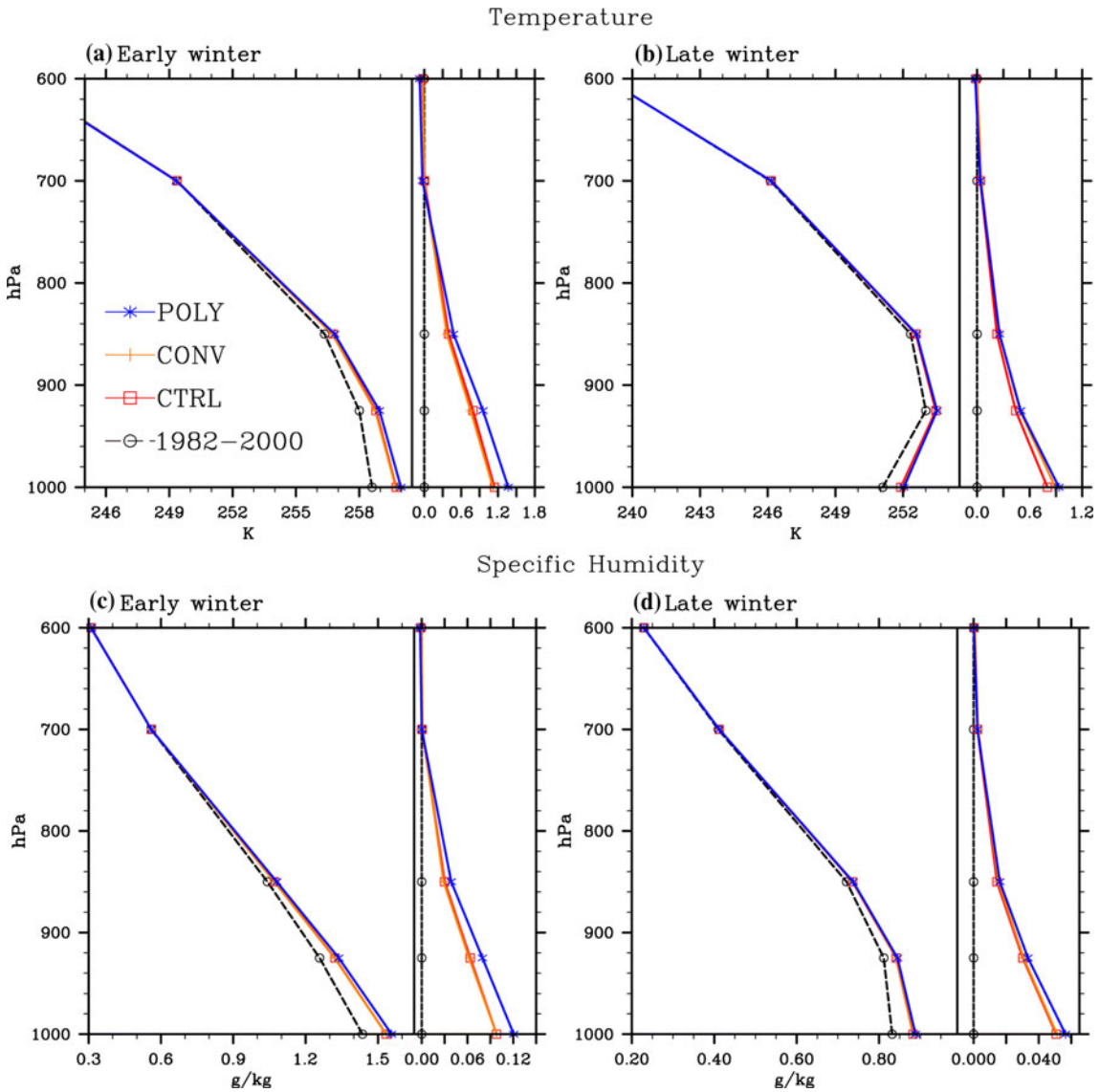

Fig. 7 Vertical profiles in temperature and specific humidity averaged over the Arctic Ocean (north of 67°N) in the baseline, CTRL, CONV, and POLY experiments during early and later winter (*left panel*) and their differences to the baseline experiment (*right panel*)

among the sensitivity experiments during the cold season (Fig. 6c).

In CTRL, CONV and POLY, changes in fluxes over the Arctic Ocean average to 1.09, 1.01, and 1.42 W m^{-2} for net longwave flux, 1.32, 1.19, and 1.65 W m^{-2} for sensible heat fluxes, and 1.32, 1.26, and 1.73 W m^{-2} for latent heat fluxes, respectively. Different SST conditions yield changes in all surface fluxes, and latent heat fluxes are most sensitive to SST conditions in the cold season. Among the surface flux differences between POLY and CTRL, those for latent heat fluxes are significant at the 90 % confidence level during the entire cold season. The sensible heat fluxes in October, November, and March, and the longwave fluxes in October and March are also significant at the 90 % confidence level. In contrast, most differences between CONV and CTRL are not statistically significant. The longwave fluxes in November and January and latent heat flux in October are significant at the 90 % confidence level.

3.2 Vertical structure of responses in temperature and specific humidity

The changes in surface fluxes related to SST eventually affect the vertical distributions of temperature and humidity, which, in turn, affects the atmospheric response to SIC and SST changes. Figure 7 shows the vertical profiles of temperature and specific humidity and their changes among the three experiments during early and late winter. For both periods, vertically extended warming and

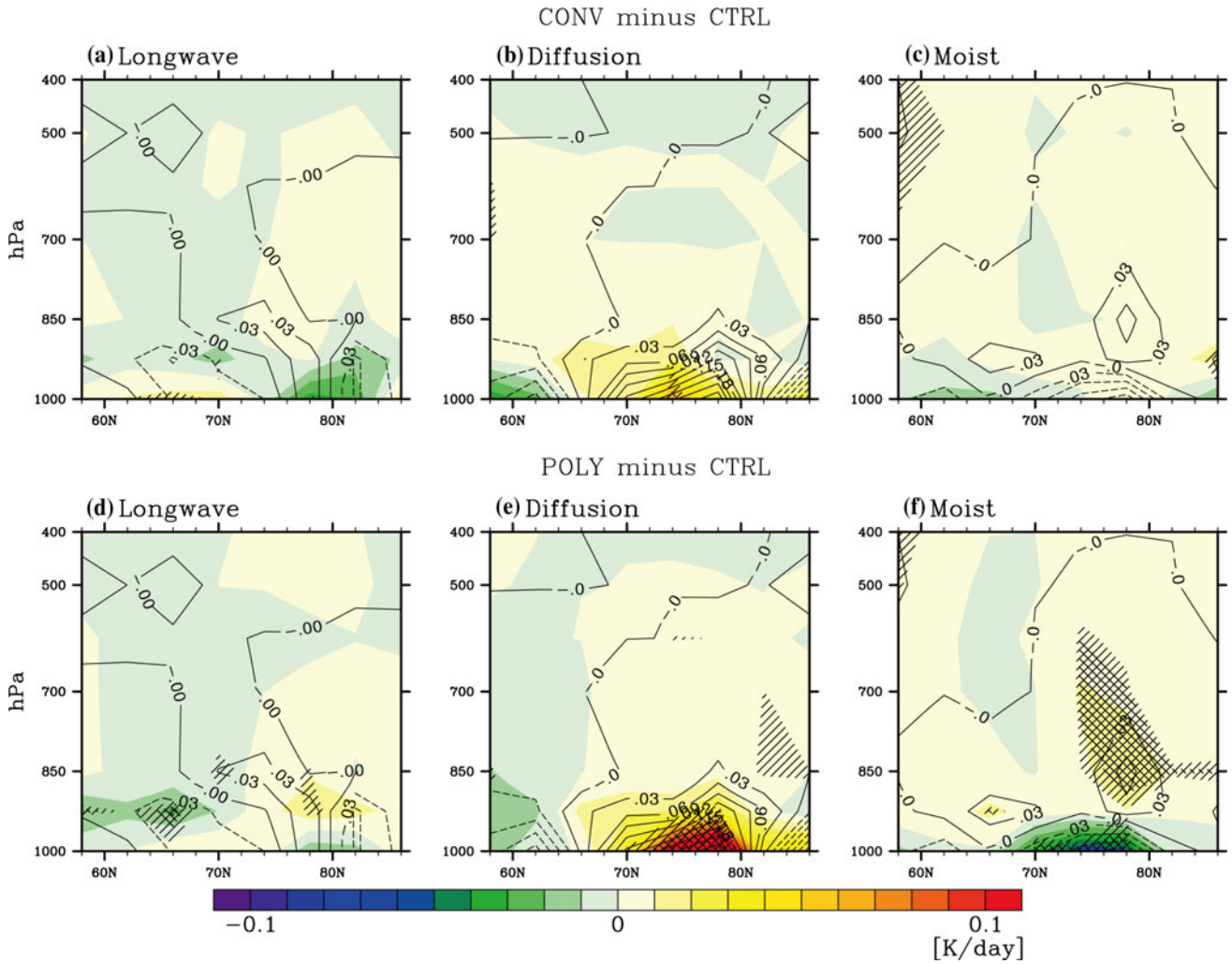

Fig. 8 Changes in zonal-averaged heating by longwave radiation, diffusion, and moist processes during the cold season. *Contour* in the figure indicates a change between CTRL and the baseline experiments, and *shade indicates* the change in CONV and POLY against CTRL. Contour interval is 0.03 K day^{-1}. Oblique and cross regions indicate that surface fluxes are significant at the 90 and 95 % confidence level, respectively

moistening are commonly found in all three sensitivity experiments. The effects of surface-induced warming and moistening on lower troposphere are larger with warmer SSTs. CTRL and CONV generate similar magnitudes of warming and moistening near the surface compared to the baseline experiment, and POLY generates warming and moistening greater than the other two experiments. During late winter, CONV also generates lower tropospheric warming greater than CTRL (Fig. 7b) with larger surface flux differences (Fig. 6).

Near-surface warming in the sea-ice reduced experiments is linked mainly to longwave radiation and sensible heat fluxes. First, longwave radiation flux from the surface is greater in MSR (Fig. 5a, d) and possibly warms the lower troposphere if the atmosphere absorbs the longwave flux. Over the Arctic, this effect of longwave flux can be stronger near the surface because of the abundance of longwave-absorbing low-cloud cover that reemits longwave radiation to the surface during the cold season (Curry et al. 1996). Figure 8a, d show longwave radiative heating at troposphere based on the SST change: CTRL generates larger longwave radiative heating over the Arctic region than baseline experiment (contour). CONV induces rather cooling compared to CTRL, and POLY induces weaker warming than CTRL (shade). Meanwhile, the difference in longwave radiative heating at lower troposphere between CONV (POLY) and CTRL is relatively weak compared to heating by other processes (Fig. 8). This may have been caused by seasonal variations in the Arctic longwave radiation; longwave radiative heating in lower troposphere is effective only during early winter due to extremely cold conditions at the near surface during middle and late winters (Fig. 6a). In addition, longwave radiative heating in the lower troposphere does not represent the only effect

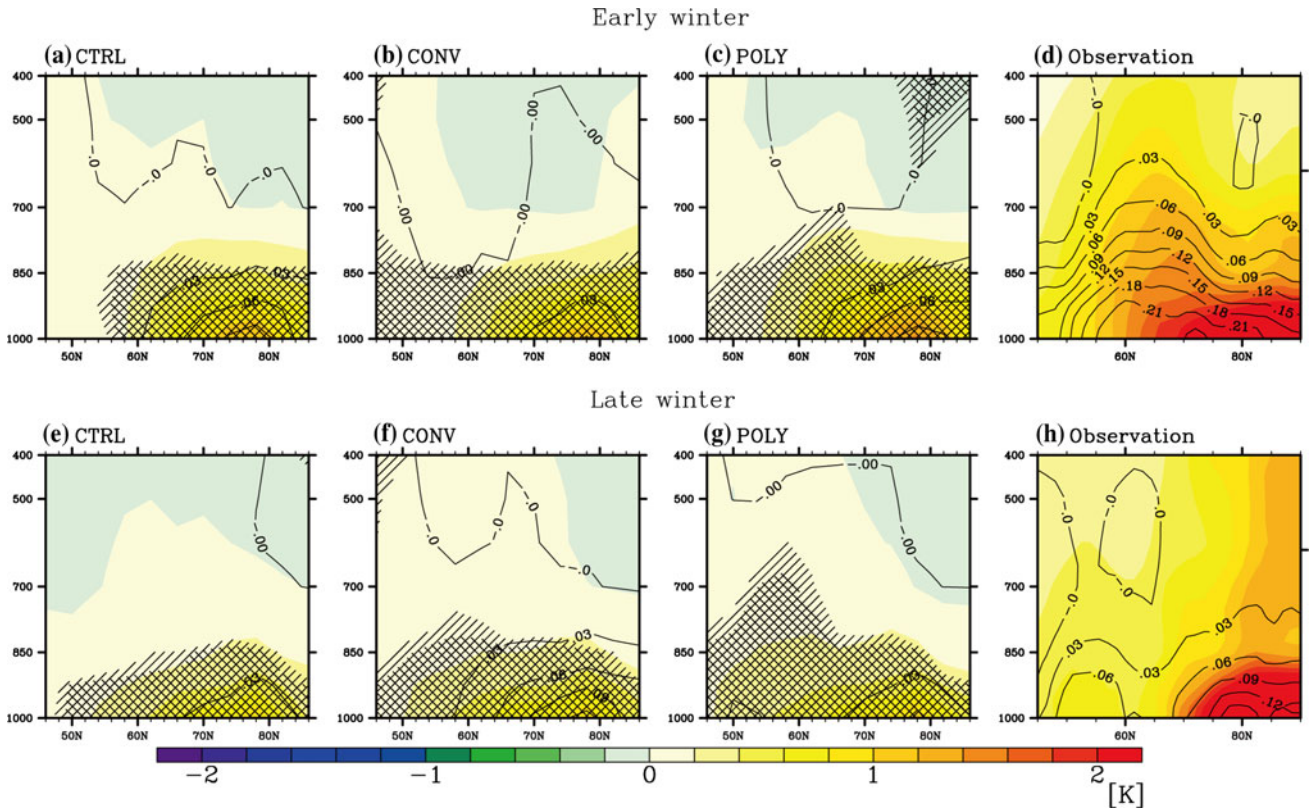

Fig. 9 Changes in zonal-averaged temperature (*shade*) and specific humidity (*contour*) during early winter (October–November–December) and late winter (January–February–March) from CTRL, CONV, and POLY experiments compared to the baseline experiment. Oblique and cross regions indicate that surface fluxes are significant at the 90 and 95 % confidence level, respectively; **d**, **h** changes in the same variables for the periods 2006–2010 and 1982–2000 from the ERA-Interim data. Contour interval is 0.03 g kg^{-1}

of longwave emissions at the surface. Because it presents the difference in longwave radiative heating in equilibrium state, longwave radiative heating results from the total effects of factors that contribute to the temperature change in the lower troposphere. Thus, the effect of change in longwave radiation at surface could be underestimated in Fig. 8a, d.

Turbulent heat diffusion in lower troposphere below 850 hPa over 70°–80°N suggests that changes in sensible heat fluxes mainly contribute to the near-surface warming (Fig. 8b, e). CTRL induces greater diffusive heating in the lower troposphere than the baseline experiment. CONV generates greater diffusive heating than CTRL, and POLY generates even greater heating than CONV. In particular, diffusive heating effects associated with different SST conditions appear to induce stronger lower atmospheric warming, as compared to the effects from longwave radiation. The difference in sensible heat flux among our experiments became larger during late winter (Fig. 6b) and it appears that the different vertical temperature profiles between early and late winter, especially shown in the difference between CTRL and CONV, might be influenced by sensible heat flux (Fig. 7a, b).

POLY simulates cooling near the surface and heating in the troposphere by moist processes that is the largest and most significant among experiments (Fig. 8f). In particular, tropospheric heating via moist processes over MSR (70°–80°N) in POLY reaches around the 500 hPa level, much higher when compared to the altitude in CONV (Fig. 8c). This vertical extension of heating by moist processes should be affected by the strengthened vertical moisture transport such as shallow convection. Large increases in the surface fluxes and associated warming and moistening induces a decrease in static stability and thickening of the planetary boundary layer. The decrease in static stability occurs through an enhanced vertical mixing of heat and moisture that, consequently, contributes to warming and moistening in the mid-troposphere. This destabilization effect associated with the increase in surface fluxes has been suggested by observational relationships between an increase in mid-level cloud cover and a decrease in SIC during early winter (Schweiger et al. 2008).

In addition to affecting vertical propagation, warmer SST conditions over MSR can spread warming and moistening further into the mid-latitudes, even under the same sea-ice condition. Figure 9 shows a vertical cross-

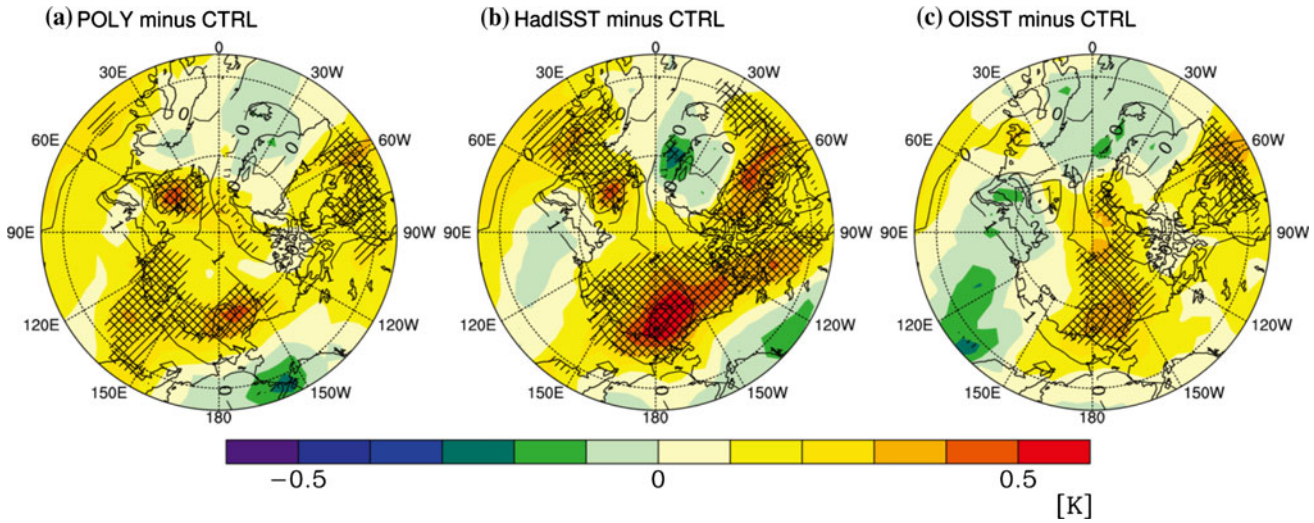

Fig. 10 Change in surface air temperature from CTRL compared to the baseline experiment (*contour*), and changes in **a** POLY, **b** HadISST over the MSR, and **c** OISSTv2 over the MSR compared to CTRL (*shade*) during the cold season. Contour interval is 0.5 K. Oblique and cross regions indicate that surface air temperature response is significant at the 90 and 95 % confidence level, respectively

section of changes in the zonal-averaged temperature (shade) and specific humidity (contours) during early and late winter for each method. It also shows observational changes. As SST becomes warmer from CTRL to POLY, warming reaches a high altitude and spreads farther south to mid-latitudes, with a corresponding change in specific humidity. In particular, the SST condition in POLY leads to warming and moistening even to the mid-latitudes as south as 45°N (Fig. 9c, g). According to ERA-Interim, warming and moistening over the high latitudes, particularly amplified warming and moistening over the Arctic, occur between the cold seasons for 2006–2010 and 1982–2000 (Fig. 9d, h). Therefore, the strong warming and moistening over the Northern Hemisphere in POLY, are closest to the recent observed changes in the Arctic and high-latitude regions. In particular, among the experiments, POLY simulates well the vertically and horizontally expanded warming during both early and late winters as captured in ERA-Interim data (Fig. 9c, g). It has been suggested that these changes in the lower troposphere is linked closely with recent drastic sea-ice melt (Screen and Simmonds 2010a); the present results support this linkage.

4 Summary and discussion

Sensitivity of atmospheric warming in response to the SST for reduced SIC in the Arctic Ocean has been examined. It has been found that temperature and moisture responses in the lower troposphere over the Arctic is sensitive to even a small amount of SST changes under the same sea-ice condition. Warmer SSTs generate substantially stronger warming near the surface, which expands vertically and horizontally compared to colder SST conditions with the same SIC. Surface heat fluxes play crucial roles in shaping these different atmospheric responses. Longwave radiation and sensible and latent heat fluxes perceptively respond to different SST conditions. Averaged over the entire cold season, latent and sensible heat fluxes are more responsible for altered atmospheric responses than longwave radiation. In particular, distribution of atmospheric heating into diffusive and condensational processes implies that sensible heat fluxes affect near-surface warming, and latent heat fluxes affect the warming in the mid-troposphere above 800 hPa. Static stability is decreased, and the air-column expands vertically due to warming and moistening in the lower troposphere.

This study suggests that the SST field in POLY may be most suitable for examining the effect of sea-ice change on the climate over the Arctic and surrounding regions as the results in POLY compares most closely with observations based on recent observational changes and in terms of larger impact on the atmosphere, vertically and horizontally. Thus, the SST adjusting methodology used in POLY can be recommended for examining the effect of sea-ice condition changes, including realistic and artificial changes.

To address the validity of the polynomial fitting method more clearly, we have conducted additional experiments using observed and prescribed SSTs and comparing results with POLY (Fig. 10). For comparison, two different SST conditions, HadISST and OISSTv2, have been used over MSR. Comparison of the mean atmospheric surface air temperature response to the SST difference for the two periods (2006–2010 vs 1982–2000) against HadISST,

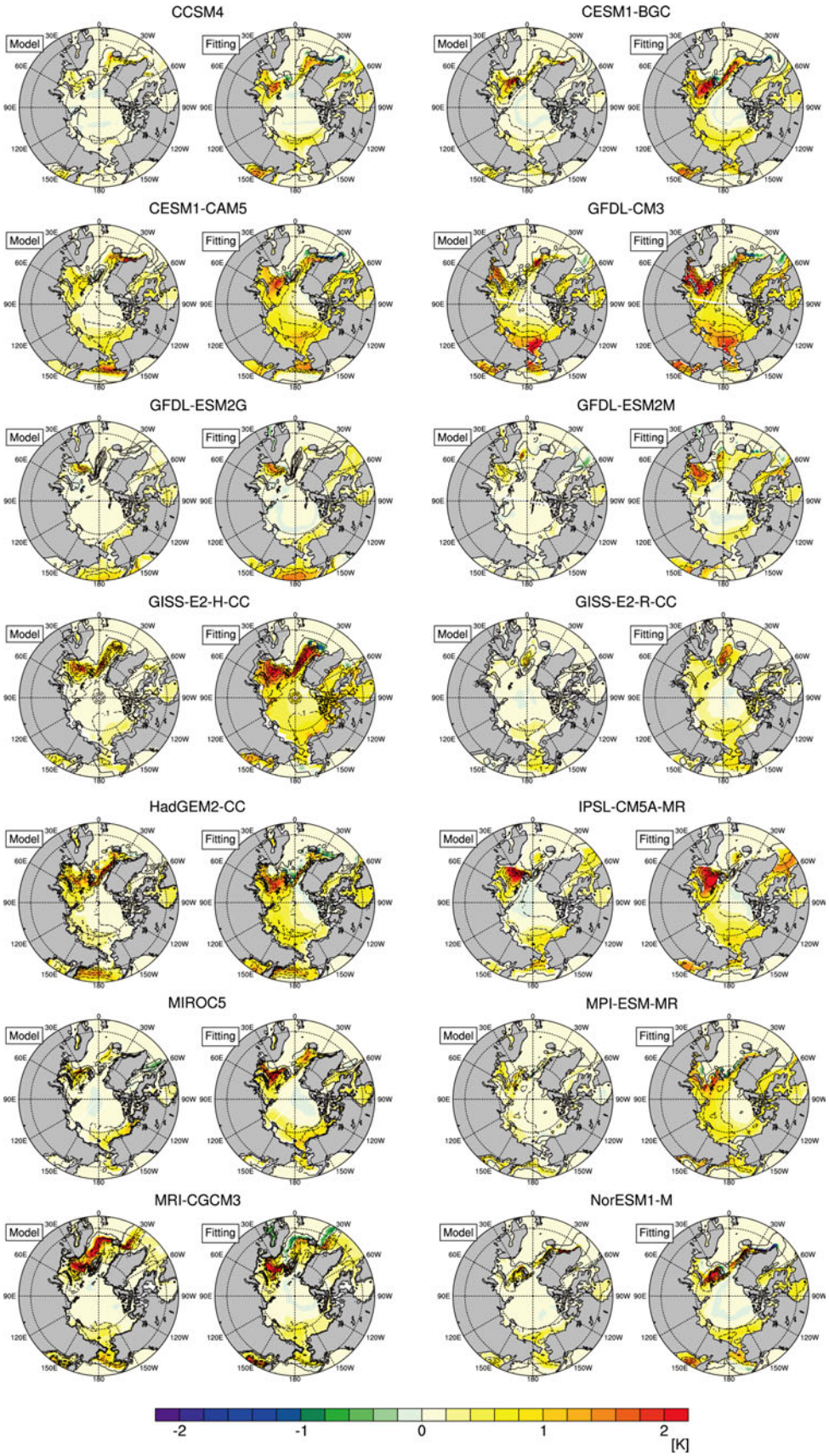

Fig. 11 Comparisons between simulated SST (model; *left figure* in *each panel*) and adjusted SST by polynomial fitting with SIC change (fitting; *right figure* in *each panel*) among 14 model results with future experiment of the RCP4.5 scenario in the fifth phase of the Climate Model Intercomparison Project. Model differences are calculated with simulated SSTs averaged for 2051–2055 and simulated SSTs averaged for 2006–2010. Fitting differences are calculated with fitted SSTs by using polynomial coefficients in the POLY method, SIC values averaged for 2051–2055 and simulated SSTs averaged for 2006–2010. *Shading* indicates sea surface temperature, and *contour* indicates sea-ice concentration with an interval of 0.1

POLY can capture qualitatively similar features, supporting the use of the polynomial fitting method (Fig. 10a, b). Rather unexpectedly, the SAT response from OISSTv2 is significantly different than that from HadISST (Fig. 10b, c). These results show that atmospheric circulation responses sensitively to small SST changes in the Arctic Ocean. It is also noted that the quality of SST observations over MSR is poor in both products and also is subjected to statistical fitting using slightly different methods (Appendix B in Rayner et al. (2003)).

The polynomial fitting method can be more useful for studies that do not use observed SST data, e.g., examining certain sea-ice melting trends on the paleo- or future climates. To examine the usability of the POLY method for future climate projection studies, we have applied our polynomial fitting coefficients to 14 model results from future experiments of RCP 4.5 scenarios in the fifth phase of the Climate Model Intercomparison Project (CMIP5). We have generated SST conditions by applying the polynomial coefficients to SIC differences between 2051–2055 and 2006–2010, and compared the generated SSTs with simulated SSTs (Fig. 11). As shown in the figure, the polynomial fitting method successfully reproduces the simulated SST distribution well in the sea-ice retreated region. The method also well captures the SST warming pattern in most of these models, although the estimated SST is slightly warmer than the simulated ones. Among the models, the estimation method gives the best match for GFDL-CM3, GFDL-ESM2G, MIROC5, MRI-CGCM3, and NorESM1-M.

Warming and moistening responses in troposphere in our study, even in POLY, are still weaker than the observed (see Fig. 9), basically due to the difference in internal variability based on the differences in the averaging periods for the observed and simulated records. Nevertheless, this can occur if recent tropospheric warming and moistening over the Arctic is induced by additional factors other than sea-ice retreat. For example, heat and moisture can be transported from the lower latitudes to the Arctic by atmospheric and oceanic circulations that also contribute to Arctic warming and moistening (Alexeev et al. 2005; Chung and Räisänen 2011; Graversen et al. 2008). Perhaps, given the weak responses obtained in this study compared to observations, contributions from other factors are larger. This situation can be explored in additional experiments using the observed global SST conditions for 2006–2010, which can replicate well the recent vertical warming structure that extends to the upper troposphere (not shown). This result also implies that there can be another important factor, in addition to melting sea-ice, which contributes to the recently observed tropospheric warming over the Arctic. The SST condition over middle or lower latitudes can be one such factor.

Acknowledgments The authors sincerely thank the two anonymous reviewers for carefully reading the earlier version of the manuscript and giving us a number of useful comments and suggestions. We also thank Jinwon Kim for his suggestions and comments on improving manuscript and Jung Choi for preparing CMIP5 dataset used in this study. We acknowledge the World Climate Research Programme's Working Group on Coupled Modelling, which is responsible for CMIP5. S.-Y. Jun specially thanks the Korea Institute of Atmospheric Prediction Systems (KIAPS), S.-Y. Jun's current affiliation, supporting modelling work for this study. This work was funded by the Korea Meteorological Administration Research and Development Program under Grant CATER 2012-3061 (PN13010) and "Climate Change Correspondence R&D Program" of Korea Ministry of Environment. This work was also supported by the Supercomputing Center/Korea Institute of Science and Technology Information with supercomputing resources including technical support (KSC-2012-G3-2).

References

Alexander MA, Bhatt US, Walsh JE, Timlin MS, Miller JS, Scott JD (2004) The atmospheric response to realistic Arctic sea ice anomalies in an AGCM during winter. J Climate 17:890–905

Alexeev VA, Langen PL, Bates JR (2005) Polar amplification of surface warming on an aquaplanet in "ghost forcing" experiments without sea ice feedbacks. Clim Dyn 24:655–666

Budikova D (2009) Role of Arctic sea ice in global atmospheric circulation: a review. Global Planet Change 68:149–163

Chung CE, Räisänen P (2011) Origin of the Arctic warming in climate models. Geophys Res Lett 38:L21704. doi:10.21029/22011gl049816

Collins WD, Rasch P, Boville B, Hack J, McCaa J, Williamson D, Kiehl J, Briegleb B, Bitz C, Lin S-J, Zhang M, Dai Y (2004) Description of the NCAR community atmosphere model (CAM 3.0): NCAR/TN-464 + STR NCAR technical note. National Center for Atmospheric Research, Boulder, Colorado, p 226

Collins WD, Bitz CM, Blackmon ML, Bonan GB, Bretherton CS, Carton JA, Chang P, Doney SC, Hack JJ, Henderson TB, Kiehl JT, Large WG, McKenna DS, Santer BD, Smith RD (2006) The community climate system model version 3 (CCSM3). J Climate 19:2122–2143

Comiso JC, Parkinson CL, Gersten R, Stock L (2008) Accelerated decline in the Arctic Sea ice cover. Geophys Res Lett 35:L01703. doi:10.01029/02007gl031972

Curry JA, Rossow WB, Randall D, Schramm JL (1996) Overview of Arctic cloud and radiation characteristics. J Climate 9:1731–1764

Dee DP, Uppala S (2009) Variational bias correction of satellite radiance data in the ERA-Interim reanalysis. Q J Roy Meteor Soc 135:1830–1841

Deser C, Magnusdottir G, Saravanan R, Phillips A (2004) The effects of North Atlantic SST and sea ice anomalies on the winter circulation in CCM3. Part II: direct and indirect components of the response. J Climate 17:877–889

Deser C, Tomas R, Alexander M, Lawrence D (2010) The seasonal atmospheric response to projected Arctic sea ice loss in the late twenty-first century. J Climate 23:333–351

Dethloff K, Rinke A, Benkel A, Koltzow M, Sokolova E, Saha SK, Handorf D, Dorn W, Rockel B, von Storch H, Haugen JE, Roed LP, Roeckner E, Christensen JH, Stendel M (2006) A dynamical link between the Arctic and the global climate system. Geophys Res Lett 33:L03703. doi:10.01029/02005gl025245

Francis JA, Chan WH, Leathers DJ, Miller JR, Veron DE (2009) Winter Northern Hemisphere weather patterns remember summer Arctic sea-ice extent. Geophys Res Lett 36:L07503. doi:10.01029/02009gl037274

Gerdes R (2006) Atmospheric response to changes in Arctic sea ice thickness. Geophys Res Lett 33:L18709. doi:10.11029/12006gl027146

Graversen RG, Mauritsen T, Tjernstrom M, Kallen E, Svensson G (2008) Vertical structure of recent Arctic warming. Nature 451:53–56

Hack J, Caron J, Danabasoglu G, Oleson K (2006) CCSM-CAM3 climate simulation sensitivity to changes in horizontal resolution. J Climate 19:2267–2289

Herman GF, Johnson WT (1978) Sensitivity of the general circulation to Arctic sea ice boundaries—numerical experiment. Mon Weather Rev 106:1649–1664

Honda M, Inoue J, Yamane S (2009) Influence of low Arctic sea-ice minima on anomalously cold Eurasian winters. Geophys Res Lett 36:Artn L08707. doi:10.01029/02008gl037079

IPCC CC (2007) The physical science basis. Contribution of working group I to the fourth assessment report of the intergovernmental panel on climate change. Cambridge University Press, Cambridge, p 996

Kiehl JT, Shields CA, Hack JJ, Collins WD (2006) The climate sensitivity of the community climate system model version 3 (CCSM3). J Climate 19:2584–2596

Kinnard C, Zdanowicz CM, Fisher DA, Isaksson E, de Vernal A, Thompson LG (2011) Reconstructed changes in Arctic sea ice over the past 1,450 years. Nature 479:509–512

Magnusdottir G, Deser C, Saravanan R (2004) The effects of North Atlantic SST and sea ice anomalies on the winter circulation in CCM3. Part I: main features and storm track characteristics of the response. J Climate 17:857–876

Meehl G, Covey C, Delworth T, Latif M, McAvaney B, Mitchell J, Stouffer R, Taylor K (2007) The WCRP CMIP3 multi-model dataset: a new era in climate change research. B Am Meteorol Soc 88:1383–1394

Murray RJ, Simmonds I (1995) Responses of climate and cyclones to reductions in Arctic winter sea-ice. J Geophys Res Oceans 100:4791–4806. doi:10.1029/4794JC02206

Newson RL (1973) Response of a general circulation model of atmosphere to removal of Arctic ice-cap. Nature 241:39–40

Overland JE, Wang MY (2010) Large-scale atmospheric circulation changes are associated with the recent loss of Arctic sea ice. Tellus A 62:1–9

Petoukhov V, Semenov VA (2010) A link between reduced Barents-Kara sea ice and cold winter extremes over northern continents. J Geophys Res Atmos 115:D21111. doi:10.21029/22009jd013568

Rayner NA, Parker DE, Horton EB, Folland CK, Alexander LV, Rowell DP, Kent EC, Kaplan A (2003) Global analyses of sea surface temperature, sea ice, and night marine air temperature since the late nineteenth century. J Geophys Res 108:4407. doi:10.1029/2002JD002670

Reynolds RW, Rayner NA, Smith TM, Stokes DC, Wang WQ (2002) An improved in situ and satellite SST analysis for climate. J Climate 15:1609–1625

Rind D, Healy R, Parkinson C, Martinson D (1995) The role of sea ice in 2 $\times$ CO2 climate model sensitivity. Part I: the total influence of sea ice thickness and extent. J Climate 8:449–463

Schweiger AJ, Lindsay RW, Vavrus S, Francis JA (2008) Relationships between Arctic sea ice and clouds during autumn. J Climate 21:4799–4810

Screen JA, Simmonds I (2010a) The central role of diminishing sea ice in recent Arctic temperature amplification. Nature 464:1334–1337

Screen JA, Simmonds I (2010b) Increasing fall-winter energy loss from the Arctic Ocean and its role in Arctic temperature amplification. Geophys Res Lett 37:L16707. doi:10.11029/12010GL044136

Screen JA, Simmonds I, Deser C, Tomas R (2012) The atmospheric response to three decades of observed Arctic sea ice loss. J Climate 26:1230–1248

Seierstad IA, Bader J (2009) Impact of a projected future Arctic Sea Ice reduction on extratropical storminess and the NAO. Clim Dyn 33:937–943

Semmler T, McGrath R, Wang S (2012) The impact of Arctic sea ice on the Arctic energy budget and on the climate of the Northern mid-latitudes. Clim Dyn 39:2675–2694

Singarayer JS, Valdes PJ, Bamber JL (2005) The atmospheric impact of uncertainties in recent Arctic sea ice reconstructions. J Climate 18:3996–4012

Singarayer JS, Bamber JL, Valdes PJ (2006) Twenty-first-century climate impacts from a declining Arctic sea ice cover. J Climate 19:1109–1125

Stroeve JC, Serreze MC, Holland MM, Kay JE, Malanik J, Barrett AP (2012) The Arctic's rapidly shrinking sea ice cover: a research synthesis. Climatic Change 110:1005–1027

Warshaw M, Rapp RP (1973) An experiment on the sensitivity of a global circulation model. J Appl Meteorol Clim 12:43–49

Winton M, Takahashi K, Held IM (2010) Importance of ocean heat uptake efficacy to transient climate change. J Climate 23:2333–2344